Please cite this article in press as: Adil et al., hPSC-Derived Striatal Cells Generated Using a Scalable 3D Hydrogel Promote Recovery in a Huntington Disease Mouse Model, Stem Cell Reports (2018), https://doi.org/10.1016/j.stemcr.2018.03.007

Stem Cell Reports
Article

ISSCR

OPEN ACCESS

hPSC-Derived Striatal Cells Generated Using a Scalable 3D Hydrogel Promote Recovery in a Huntington Disease Mouse Model

Maroof M. Adil,[1] Thomas Gaj,[2] Antara T. Rao,[3] Rishikesh U. Kulkarni,[4] Christina M. Fuentes,[2] Gokul N. Ramadoss,[1] Freja K. Ekman,[4] Evan W. Miller,[3,4,5] and David V. Schaffer[1,2,3,5,*]

[1]Department of Chemical and Biomolecular Engineering, University of California, Berkeley, Berkeley, CA 94720, USA
[2]Department of Bioengineering, University of California, Berkeley, Berkeley, CA 94720, USA
[3]Department of Molecular and Cell Biology, University of California, Berkeley, Berkeley, CA 94720, USA
[4]Department of Chemistry, University of California, Berkeley, Berkeley, CA 94720, USA
[5]The Helen Wills Neuroscience Institute, University of California, Berkeley, Berkeley, CA 94720, USA
*Correspondence: schaffer@berkeley.edu
https://doi.org/10.1016/j.stemcr.2018.03.007

SUMMARY

Huntington disease (HD) is an inherited, progressive neurological disorder characterized by degenerating striatal medium spiny neurons (MSNs). One promising approach for treating HD is cell replacement therapy, where lost cells are replaced by MSN progenitors derived from human pluripotent stem cells (hPSCs). While there has been remarkable progress in generating hPSC-derived MSNs, current production methods rely on two-dimensional culture systems that can include poorly defined components, limit scalability, and yield differing preclinical results. To facilitate clinical translation, here, we generated striatal progenitors from hPSCs within a fully defined and scalable PNIPAAm-PEG three-dimensional (3D) hydrogel. Transplantation of 3D-derived striatal progenitors into a transgenic mouse model of HD slowed disease progression, improved motor coordination, and increased survival. In addition, the transplanted cells developed an MSN-like phenotype and formed synaptic connections with host cells. Our results illustrate the potential of scalable 3D biomaterials for generating striatal progenitors for HD cell therapy.

INTRODUCTION

Huntington disease (HD) is a currently incurable, inherited neurological disorder characterized by irregular and involuntary movements of the muscles and progressive loss of cognitive ability (Walker, 2007). HD is caused by the expansion of a CAG trinucleotide repeat within exon 1 of the huntingtin (HTT) gene, which leads to the production of a toxic mutant protein that kills striatal medium spiny neurons (MSNs) and also affects the surrounding regions of the brain (Ehrlich, 2012). Current treatment options for HD offer only early stage symptomatic relief and do not affect disease progression. HD patients thus experience a declining quality of life following disease onset and eventually succumb to the disease ~20 years after its initial manifestation (Foroud et al., 1999), and effective treatments for HD are therefore urgently needed.

Cell replacement therapy (CRT), an approach in which cells are transplanted to replenish damaged or dysfunctional tissue, offers promise for treating HD. For example, seminal clinical trials (Bachoud-Lévi et al., 2006; Gallina et al., 2010) demonstrated slowed cognitive deterioration and moderately improved motor function in HD patients following the transplantation of fetal-derived neural tissue. While both promising and pioneering, these strong proof-of-concept efforts were ultimately unable to halt disease progression, perhaps due to a lack of effective donor cell sources and the transplantation of poorly defined cell populations (Rosser and Bachoud-Lévi, 2012). Fortunately, human pluripotent stem cells (hPSCs), with their hallmark capacities for unlimited self-renewal and broad differentiation, represent a potentially unlimited source of tissue for cell therapy to enable CRT for HD to proceed. In important prior work, striatal MSNs (Arber et al., 2015; Aubry et al., 2008; Delli Carri et al., 2013; Ma et al., 2012) were generated from hPSCs by modulating the Sonic Hedgehog (SHH) and/or WNT signaling pathways, which enabled subsequent application of these cells toward CRT in HD. That said, transplantation of these striatal populations into chemically lesioned rodent models of HD led to mixed therapeutic outcomes (Arber et al., 2015; Delli Carri et al., 2013; Ma et al., 2012), including graft overgrowth (Aubry et al., 2008; Delli Carri et al., 2013; Ma et al., 2012) and only partial functional recovery. Therefore, there has been some important progress, although general methods to efficiently generate safe, transplantable cells capable of alleviating disease symptoms are still needed.

In general, three-dimensional (3D) biomaterial scaffolds potentially offer a biomimetic environment that can enhance the derivation of specific cell populations from hPSCs (Pampaloni et al., 2007). Several materials have been previously utilized for pluripotent stem cell culture and differentiation, including hyaluronic acid and alginate (Gerecht et al., 2007; Kraehenbuehl et al., 2011; Lei and Schaffer, 2013). In addition, we have proposed 3D biomaterial culture as a scalable platform for stem cell expansion and differentiation (Lei and Schaffer, 2013) to satisfy the large-scale manufacturing demands needed for

Please cite this article in press as: Adil et al., hPSC-Derived Striatal Cells Generated Using a Scalable 3D Hydrogel Promote Recovery in a Huntington Disease Mouse Model, Stem Cell Reports (2018), https://doi.org/10.1016/j.stemcr.2018.03.007

clinical translation of cell therapy. Previously, we used a fully defined, biocompatible, thermoresponsive, and scalable poly(N-isopropylacrylamide)-co-polyethylene glycol (PNIPAAm-PEG) 3D hydrogel system to continuously and efficiently expand hPSCs for months *in vitro*, at higher expansion rates compared with other commonly used 3D materials (Lei and Schaffer, 2013). This thermoreversible material is a liquid below room temperature and forms a gel at 37°C, which enables rapid, non-enzymatic, stress-free encapsulation and recovery of cells by simple temperature cycling between 4°C and 37°C, making it an ideal 3D platform from which to harvest fragile neuronal cells. We also previously demonstrated that hPSC-derived dopaminergic neuronal progenitors (Lei and Schaffer, 2013), midbrain dopaminergic neurons (Adil et al., 2017a), and oligodendrocyte progenitors (Rodrigues et al., 2017) could be generated in this PNIPAAm-PEG system.

Here, we engineered this scalable, thermoresponsive biomaterial platform to develop a protocol for producing hPSC-derived striatal progenitors that rapidly attain an MSN-like phenotype. We show that striatal progenitors generated in 3D promote functional recovery and extend survival following transplantation into a progressively degenerating transgenic mouse model of HD. Importantly, grafted cells innervated the host tissue and formed synaptic connections with endogenous neurons. Our results therefore indicate that hPSC-derived striatal cells generated in 3D have potential for treating HD.

RESULTS

Modulating Wnt and SHH Signaling to Generate Striatal Progenitors in a 3D Hydrogel

We investigated whether hPSC-derived striatal progenitors could be efficiently generated within a 3D biomaterial. During natural development, striatal MSNs arise from lateral ganglionic eminence (LGE) striatal progenitors in the telencephalon within a region specified anteroposteriorly (AP) by opposing Dickkopf related protein 1 (DKK1) and WNT signaling, and dorsoventrally by WNT and SHH signaling (Figure 1A). Previously, using approaches inspired by natural development, dopamine, and cyclic AMP (cAMP) regulated neuronal phosphoprotein (DARPP32)$^+$ neurons were generated from hPSCs using SHH modulation alone (Ma et al., 2012) or in combination with the WNT antagonist DKK1 (Delli Carri et al., 2013). WNT inhibition, in particular, yielded MSNs transcriptionally similar to those present in the brain. Moreover, several other non-MSN neuronal lineages (Kirkeby et al., 2012; Kriks et al., 2011) were previously generated using Neurobasal medium, a formulation that enhances neuronal culture compared with other media (Brewer et al., 1993), such as DMEM. Hence, we designed three different MSN differentiation media conditions (M1, M2, and M3) to investigate the combinatorial effect of DKK1, SHH, and Neurobasal medium on generating MSN-like cells in a thermoreversible PNIPAAm-PEG hydrogel (Figure 1B).

After 26 days (D26) of differentiation of H1 hESCs in the 3D biomaterial using conditions M1, M2, and M3, we used qPCR to profile the resulting cells (Figure 1C). The three conditions generated cells with equivalent levels of *CTIP2* (also known as *BCL11B*), a transcription factor essential for the formation of DARPP32$^+$ MSNs (Arlotta et al., 2008). However, we found that WNT inhibition (M2 relative to M1) increased the expression of markers found in the early LGE, namely *GSX2* and *OTX2*, and decreased the expression of both the late LGE progenitor markers *FOXP1* and *FOXP2* and the pan-neuronal marker *MAP2* (Figure 1C). WNT inhibition may thus delay differentiation in these experiments. Interestingly, inclusion of Neurobasal medium (M3) alongside WNT inhibition reversed this trend, yielding the lowest levels of *GSX2* and *OTX2* and the highest levels of *FOXP1*, *FOXP2*, and *MAP2* among the three conditions tested (Figure 1C).

Next, we investigated the potential for *in vitro* neuronal maturation of LGE (striatal) progenitors generated in 3D hydrogels using the three protocols (M1, M2, and M3). Toward this end, we harvested progenitors generated in 3D for 26 days and further cultured them on a two-dimensional (2D) laminin-coated surface for ease of staining and microscopy. Immunocytochemistry analysis at D45 revealed γ-aminobutyric acid (GABA) and CALBINDIN expression in cells generated under all three conditions (Figures 1D and 1E). Interestingly, however, WNT inhibition with DKK1, with or without Neurobasal medium, doubled the number of DARPP32$^+$ cells from 20% to 40%. Taken together, these results indicate that combining WNT inhibition and SHH activation within the 3D platform efficiently yields striatal progenitors and that Neurobasal medium accelerates the process. Thus, from this point on, striatal progenitors were differentiated using condition M3. Notably, condition M3 differs from previously established striatal differentiation conditions through the combined use of the SHH agonist PPA with WNT antagonist DKK1, and the neuron supportive base medium Neurobasal. To demonstrate broader applicability, we used this protocol to similarly differentiate H9 hESCs and 8FLVY6C2 hiPSCs (Lan et al., 2013) to striatal cells (Figure S1).

As a benchmark, we differentiated striatal progenitors on a conventional 2D platform (Matrigel-coated polystyrene) using media condition M3 (Figures S2A and S2B). Quantitative immunocytochemistry showed a steady increase in DARPP32$^+$ and CTIP2$^+$ cells from ~7% and 3%, respectively, on D25 to 22% and 31%, respectively, on D45 in 2D (Figure S2B), on par with a previous study reporting

Please cite this article in press as: Adil et al., hPSC-Derived Striatal Cells Generated Using a Scalable 3D Hydrogel Promote Recovery in a Huntington Disease Mouse Model, Stem Cell Reports (2018), https://doi.org/10.1016/j.stemcr.2018.03.007

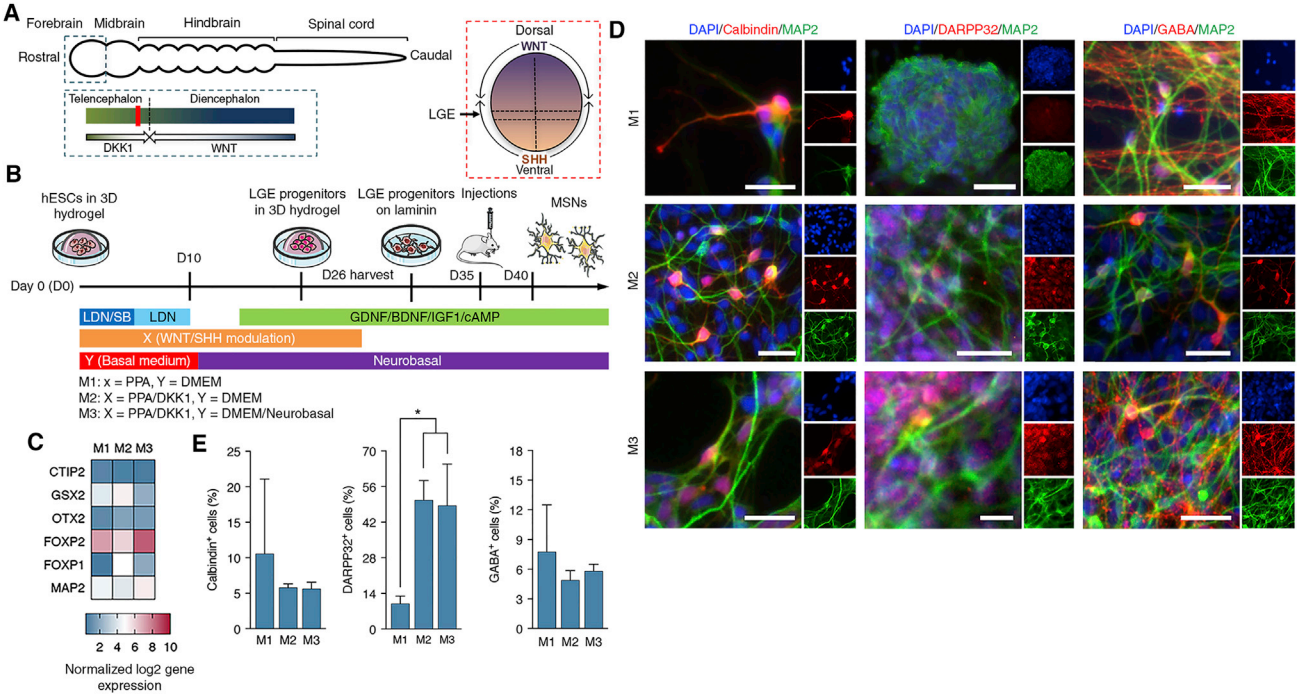

Figure 1. Optimizing MSN Differentiation in Three Dimensions

(A) Development of LGE progenitors. Antagonistic DKK1 and WNT signaling give rise to the telencephalon in the rostral forebrain (blue inset). In the posterior telencephalon (red inset), antagonistic WNT and SHH signaling produce the LGE progenitors.

(B) Schematic and media conditions for MSN differentiation optimization in three dimensions. H1 hESCs encapsulated in hydrogels were differentiated into LGE progenitors for 26 days and subsequently matured into MSNs on laminin-coated plates. Three different protocols were tested (M1, M2, and M3) with varying WNT/SHH modulation (X) and basal medium (Y).

(C) qPCR at D28 of differentiation for media conditions M1, M2, and M3, showing $\log_2$ gene expression normalized to GAPDH.

(D) Representative immunocytochemistry images at D45 for conditions M1, M2, and M3, showing CALBINDIN (red, left panels), DARPP32 (red, center panels), and GABA (red, right panels), with MAP2 (green) and nuclei labeled with DAPI (blue). Scale bars represent 20 μm.

(E) Quantification of immunocytochemistry results showing the percentage of total cells positive for DARPP32, CALBINDIN, and GABA for conditions M1, M2, and M3. Data are presented as mean ± SEM for n = 3 independent experiments. *$p < 0.05$ for unpaired t test.

~20% hPSC-derived DARPP32$^+$/CTIP2$^+$ neurons using a 2D platform with a similar protocol (Delli Carri et al., 2013). In contrast, in parallel 3D cultures at D28, we found a 7-fold higher proportion of DARPP32$^+$ and a 13-fold higher proportion of CTIP2$^+$ striatal cells ($p < 0.05$) relative to D25 2D cultures (Figure S2B). qPCR corroborated these findings and showed that common striatal MSN markers, including *DARPP32* (also known as *PPP1R1B*), *CTIP2*, *FOXG1*, *FOXP1*, and *FOXP2*, were upregulated in 3D between D28 and D45 (Figure S2C). Thus, striatal MSN-like cells were generated at a higher efficiency when starting in a 3D platform.

Striatal Progenitors Generated in 3D Mature into Striatal Neurons that Fire Action Potentials

To investigate functional maturation of the striatal neurons, striatal progenitors were generated in 3D hydrogels for 26 days and then matured on 2D laminin-coated plates, to facilitate voltage-sensitive dye-based imaging of action potentials (Kulkarni et al., 2017). Immunocytochemistry at D60 showed robust expression of the striatal MSN markers DARPP32, CTIP2, GABA, and CALBINDIN (Figures 2A–2C). Specifically, 78% of cells were MAP2$^+$ (Figure 2D), and, of these, 61% were GABA$^+$, 55% were DARPP32$^+$, 70% were CTIP2$^+$, and 46% were CALBINDIN$^+$ (Figure 2E). Importantly, the entire DARPP32$^+$ population was CTIP2$^+$, an important feature of *in vivo* MSNs (Arlotta et al., 2008; Delli Carri et al., 2013). Also, 27% of the cells expressed GFAP, a glial marker commonly expressed in differentiated hPSC cultures (Figure 2E).

An important hallmark of neuronal functionality is the capacity to fire membrane action potentials. We used a voltage-sensitive dye-based imaging platform (Kulkarni et al., 2017; Woodford et al., 2015) to monitor the membrane potential of MSNs derived from striatal progenitors. At D60, cells differentiated entirely on 2D were not active (Figure S2D). In stark contrast, at the same time point, 69% of cells that were differentiated for the first 26 days in the 3D biomaterial spontaneously fired action potentials

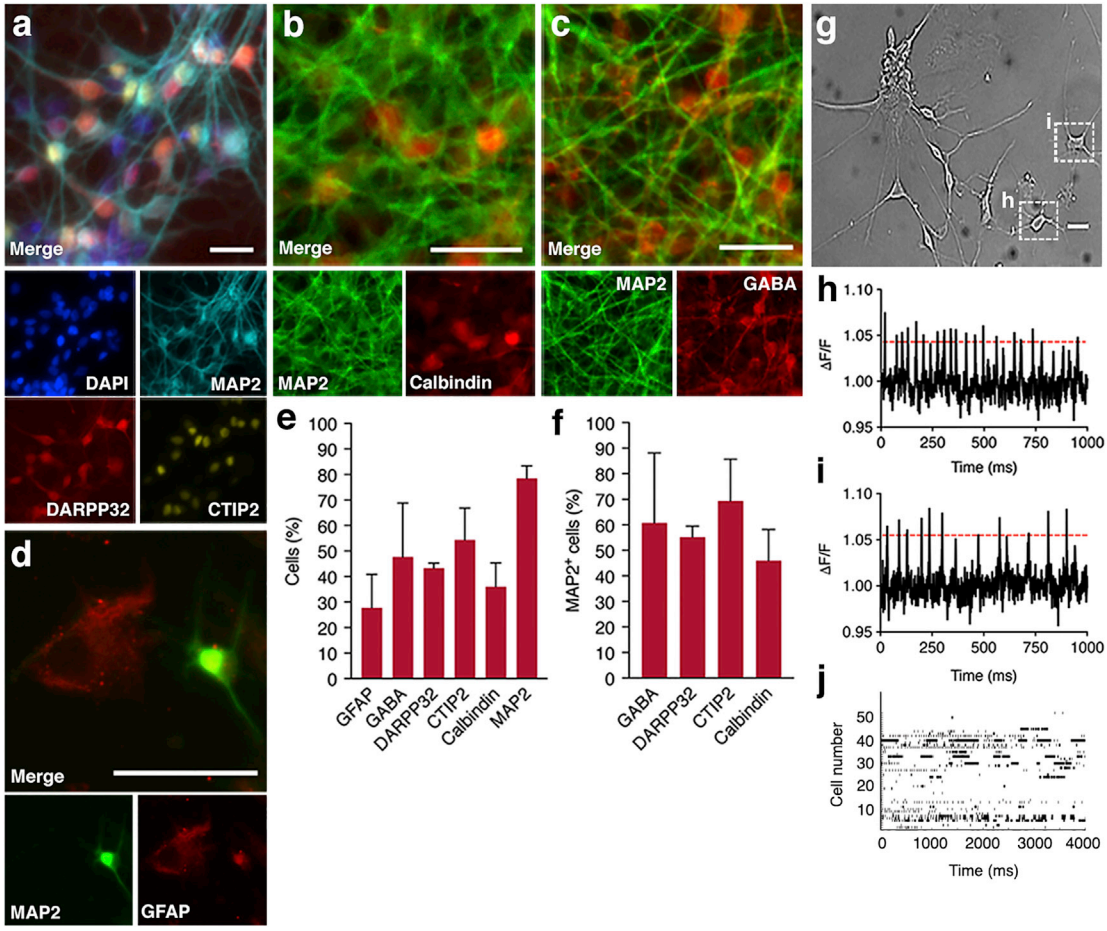

Figure 2. *In vitro* MSN Maturation and Action Potential Firing at D60

(A–D) Striatal progenitors were generated using condition M3 in 3D hydrogels for 26 days, then subsequently plated and matured on 2D laminin-coated plates until D60 for histology and live imaging analysis. Representative immunocytochemistry images showing co-expression of (A) DARPP32 (red), CTIP2 (yellow), MAP2 (cyan), and nuclei (labeled with DAPI, blue); (B) CALBINDIN (red) with MAP2 (green); (C) GABA (red) with MAP2 (green); and (D) GFAP (red) with MAP2 (green). Scale bars represent 50 μm.

(E and F) Quantification of the fraction of cells positive for markers of interest. Data are presented as mean ± SEM for n = 3 independent experiments.

(G–J) Voltage-sensitive dye-based recording of spontaneously fired action potential in striatal cultures. (G) Representative bright-field image of recorded cells. (H and I) Plots of ΔF/F versus time for cells labeled in (G). (J) Raster plot showing spiking frequencies for all recorded cells, firing and non-firing.

(Figures 2F–2I), which interestingly closely corroborated with the fraction of neurons (78% MAP2$^+$ cells) observed (Figure 2E). D60 3D-generated neurons also demonstrated evoked activity (Figure S2E). Due to the apparently slower maturation rate for MSN progenitors differentiated on 2D (Figure S2), we again looked for spiking activity at D90, and observed that 73% (statistically indistinguishable from the D60 3D-derived cells, $p = 0.73$) of 2D-derived cells spontaneously fired action potentials at this point (Figure S2F). Immunocytochemistry at D90 confirmed that the 2D-generated cells expressed DARPP32, CTIP2, GABA, and MAP2 (Figures S2G and S2H). Our results therefore indicate that early 3D culture substantially accelerates the generation of striatal progenitors and their maturation into striatal neurons, which for therapeutic application may reduce manufacturing time by rapidly generating transplant-ready cells (e.g., 49% DARPP32$^+$ cells after 28 days of differentiation), increase throughput, and reduce risk of culture loss due to contamination.

3D-Derived Striatal Progenitors Promote Functional Recovery in HD Mice

We next evaluated whether striatal progenitors generated in 3D could alleviate disease symptoms following

Please cite this article in press as: Adil et al., hPSC-Derived Striatal Cells Generated Using a Scalable 3D Hydrogel Promote Recovery in a Huntington Disease Mouse Model, Stem Cell Reports (2018), https://doi.org/10.1016/j.stemcr.2018.03.007

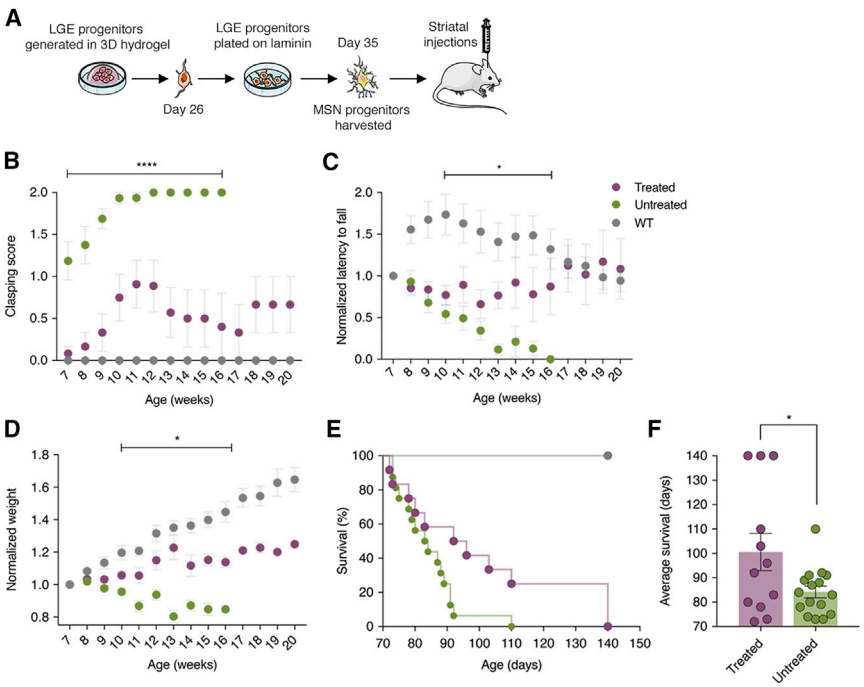

Figure 3. Transplantation of 3D-Derived Striatal Progenitors Provides Therapeutic Benefit to HD Mice

(A–D) Striatal progenitors generated in 3D hydrogels for 26 days were matured on laminin-coated surfaces for 10 days before harvest and bilateral striatal transplantation into 5-week-old R6/2 mice. Starting 2 weeks after transplantation, disease progression was monitored weekly with (B) clasping, (C) rotarod, and (D) weight change for R6/2 HD mice (purple; n = 12), control untreated HD mice (green; n = 16), and wild-type (WT) mice (gray; n = 11). ****$p < 0.0001$ and *$p < 0.05$ for one-way ANOVA with Tukey's test for multiple comparisons.

(E) Survival data shown in a Kaplan-Meier plot.

(F) Mean survival for treated (n = 12) and untreated R6/2 mice (n = 16). *$p < 0.05$ for Welch's unpaired t test.

Data are shown as means ± SEM. See also Figure S3.

transplantation into a mouse model of HD. We employed the R6/2 model of the disease (Mangiarini et al., 1996), which expresses a mutant of exon 1 of the human HTT gene containing ~120 CAG repeats. This mouse model recapitulates many fundamental aspects of HD, including chorea, tremors, and epileptic seizures (Cepeda-Prado et al., 2012; Li et al., 2005). We transplanted ~100,000 D35 striatal progenitors bilaterally into the striatum of 5-week-old R6/2 mice (Figure 3A) and evaluated animals weekly for weight loss, motor deficits (Carter et al., 1999), and clasping (Paul et al., 2014) (a dystonic posture of the hind limbs observed when mice are suspended by the tail).

As anticipated, we observed the initial signs of disease-associated clasping at 7 weeks of age in untreated mice (Figures 3B and S3A). In contrast, clasping in the treated cohort was delayed by 1 week compared with untreated animals and persisted at lower levels than the untreated group over the course of the study ($p < 0.0001$) (Figures 3B and S3A). Untreated mice also showed impaired motor function starting at 8 weeks of age, with rotarod performance continuously deteriorating for the remainder of the study (Figure 3C). On the contrary, treated mice displayed steady performance on the rotarod, and demonstrated significantly improved motor coordination relative to untreated mice after 10 weeks of age ($p < 0.05$) (Figures 3C and S3B). Furthermore, while untreated mice exhibited weight loss starting at 9 weeks, we observed no reduction in weight in any treated animal until 14 weeks of age (Figures 3D and S3C). Finally, 94% of untreated mice succumbed to disease between 10 and 13 weeks of age (Figure 3E). Remarkably, 50% of treated animals lived beyond 13 weeks of age, and furthermore four of these treated animals showed disease symptoms only after 16 weeks of age (Figure 3C) and were sacrificed between 17 and 20 weeks of age for histology (Figure 3E). Thus, transplantation of 3D-derived striatal progenitors increased survival in R6/2 mice by at least 16 days, corresponding to a ~19% increase in lifespan ($p < 0.05$) (Figure 3F). Also, it is possible that lifespan could be extended longer, but the remaining mice were sacrificed at this stage to examine graft morphology.

Implanted Cells Survive and Maintain an MSN-like Phenotype and Integrate in Host Tissue

Transplanted cells must survive and presumably integrate within the host tissue for cell therapy to effectively treat HD and other neurodegenerative diseases. We thus investigated the status of the MSN progenitor grafts in R6/2 mice 12–15 weeks post transplantation (corresponding to an overall age of 17–20 weeks) (Figure 3). Immunohistochemical analysis revealed the presence of human nuclear antigen (HNA) (Figures 4A and 4B) on DARPP32$^+$ cells. On average, ~6% of the transplanted MSN progenitors survived in the R6/2 striatum.

A hallmark of functional striatal grafts and a prerequisite for alleviating HD symptoms by cell therapy is the formation of synaptic connections between the grafted cells and

Please cite this article in press as: Adil et al., hPSC-Derived Striatal Cells Generated Using a Scalable 3D Hydrogel Promote Recovery in a Huntington Disease Mouse Model, Stem Cell Reports (2018), https://doi.org/10.1016/j.stemcr.2018.03.007

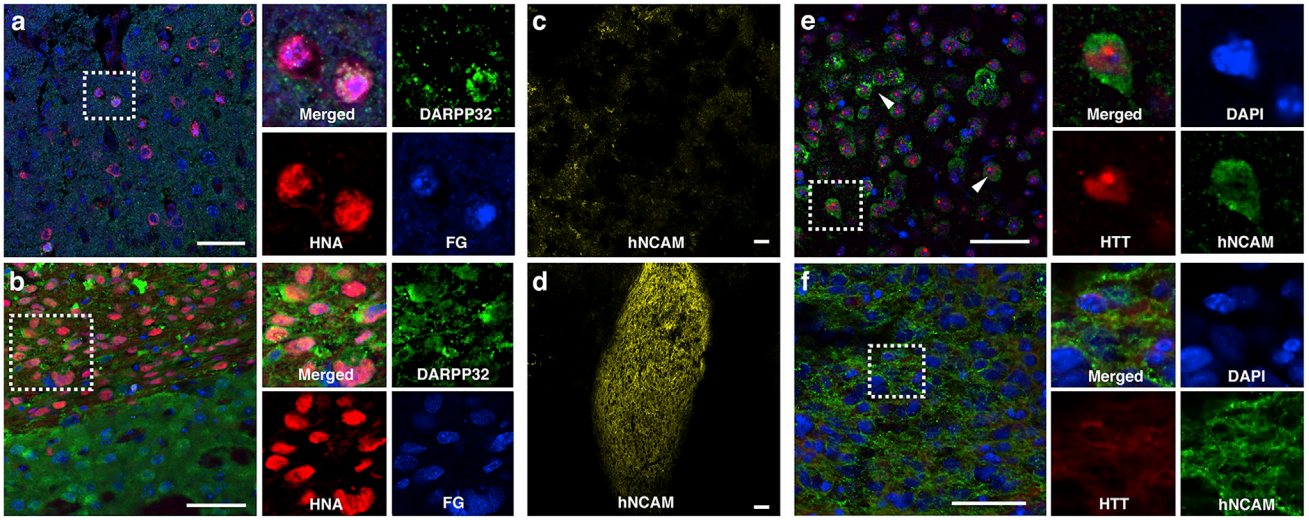

Figure 4. Survival and Integration of Grafted Human Cells

(A–D) R6/2 or wild-type mice transplanted with D35 striatal neurons were sacrificed 12–15 weeks post transplantation, corresponding with an overall age of 17–20 weeks. Representative immunohistochemistry images showing expression of HNA (red) and DARPP32 (green) in (A) R6/2 mice or (B) wild-type mice. Co-labeling with Fluorogold (FG, blue) demonstrates connectivity with the substantia nigra. hNCAM (yellow) expressing human cells in (C) sparse surviving graft in R6/2 mice or (D) robust graft in wild-type mice.

(E) Nuclear-localized HTT aggregates (red) were seen in many of the hNCAM (green) expressing human cells, some of which are indicated by white arrows, in R6/2 mice.

(F) No HTT aggregates were seen in hPSC-derived MSNs transplanted in wild-type mice.

Scale bars represent 50 μm. See also Figure S4.

the surrounding neuronal architecture (Nakao and Itakura, 2000; Rosser and Bachoud-Lévi, 2012). One of the primary targets of striatal MSN projections is the substantia nigra, and to investigate this possibility we injected the retrograde tracer Fluorogold (FG) into the substantia nigra 10 weeks after implantation. Notably, we observed retrograde FG labeling of the striatally transplanted human cells (Figures 4A and 4B), indicating that transplanted MSN progenitors innervated the endogenous host neuronal architecture and corroborating behavioral studies. Our analysis also revealed no cell overgrowth in the striatum. Previously, transplantation of ~50,000–100,000 striatal progenitors into quinolinic acid (QA) lesioned rodent brains resulted in ~3–4 million surviving cells 9–16 weeks post transplantation, indicating a high degree of cell overgrowth (Aubry et al., 2008; Delli Carri et al., 2013; Ma et al., 2012). This reported overgrowth could be due to the presence of mitotic progenitor cells in the xenograft. The lack of overgrowth seen here could stem from our transplantation of more mature, post-mitotic MSN progenitors, as indicated by the marker expression profiles identified with immunocytochemistry and qPCR (Figures 2 and 3).

Finally, to potentially explain why R6/2 animals transplanted with hPSC-derived MSNs eventually succumb to disease, we hypothesized that the progressive neurodegeneration adversely affects long-term graft viability. To test this possibility, we compared morphology and histology of hPSC-derived MSN grafts in R6/2 mice versus in healthy wild-type mice 12–15 weeks after transplantation. Interestingly, we observed that surviving grafts were smaller and sparser in R6/2 mice (Figure 4C) relative to wild-type mice (Figure 4D). Grafts in the wild-type mice were morphologically similar to previously reported grafts in non-degenerative disease models (Ma et al., 2012). This suggested that the progressively neurodegenerative environment in R6/2 mice adversely affected graft viability. To gain additional insights into a potential mechanism of eventual graft failure in R6/2 mice, we investigated HTT localization in grafted mice. Previously, transfer of mutant HTT aggregates from diseased R6/2 brain tissue has been linked to neurotoxicity and abnormal cell morphology of co-cultured healthy hPSC-derived neurons in *ex vivo* brain slices (Pecho-Vrieseling et al., 2014). Corroborating these previous *in vitro* results, we observed nuclear-localized HTT aggregates not only in R6/2 host tissue (Figure S4A) but also within transplanted human neurons in the R6/2 mice (Figure 4E). As anticipated, HTT aggregates were not observed in hPSC-derived MSNs transplanted in wild-type mice (Figure 4F) or in the wild-type host tissue (Figure S4B). This *in vivo* observation offers a potential mechanism for the eventual fate of the graft in R6/2 mice.

Please cite this article in press as: Adil et al., hPSC-Derived Striatal Cells Generated Using a Scalable 3D Hydrogel Promote Recovery in a Huntington Disease Mouse Model, Stem Cell Reports (2018), https://doi.org/10.1016/j.stemcr.2018.03.007

DISCUSSION

Robust differentiation strategies for efficiently generating striatal neurons from hPSCs have the potential to advance cell therapies for HD and other neurodegenerative disorders, and the development of scalable and efficient methods for the large-scale manufacturing of striatal neurons could help to foster their translation to the clinic. To this end, building upon prior work with stem cells and biomaterials (Aubry et al., 2008; Delli Carri et al., 2013; Lei and Schaffer, 2013; Ma et al., 2012), we designed a protocol to efficiently generate striatal populations within a thermoresponsive and scalable PNIPAAm-PEG hydrogel using fully defined conditions. We found that striatal transplantation of the resulting 3D-derived progenitors into the R6/2 mouse model of HD resulted in engrafted cells that displayed an MSN-like phenotype, innervated the host tissue and endogenous neurons, and thereby promoted functional recovery and increased survival.

Several studies have demonstrated the benefits of 3D organoid culture for generating a range of cell types from hPSCs (Chen, 2016; Lancaster et al., 2013; Yin et al., 2016), and we recently developed protocols for the efficient derivation of midbrain dopaminergic neurons in a 3D biomaterial (Adil et al., 2017a). In this study, by utilizing the SHH and WNT signaling pathways, we describe a 3D protocol that enhances rapid striatal differentiation within a biomaterial compared with a 2D control, as indicated by a higher fraction of DARPP32$^+$ cells (45% in 3D versus 22% in 2D, at D45), and spiking activity (69% of cells firing in 3D versus none in 2D, at D60). Improved differentiation within a 3D hydrogel could result from material or mechanical cues that prime stem cells for optimal differentiation (Lin et al., 2016) and/or encourage the natural production of an extracellular matrix optimal for the biomimetic development of the desired cell types (Murphy et al., 2014). Furthermore, the thermoreversible platform used here enables rapid and facile cell seeding and harvesting and may facilitate large-scale production of different cell types (Lei and Schaffer, 2013). Scalable 3D generation of functional cell types may substantially facilitate CRT, disease modeling, drug screening, and *in vitro* organogenesis.

Since striatal MSNs are the most common cell type lost during HD, several protocols for differentiating hPSCs have been pursued, each with varying degrees of efficiency and post-transplantation outcomes (Arber et al., 2015; Aubry et al., 2008; Delli Carri et al., 2013; Ma et al., 2012). However, there is no consensus on the optimal age or composition of cells at the time of transplantation for successful HD treatment. Ma et al. (2012) used SHH modulation to generate a striatal population consisting of ~70% DARPP32$^+$ cells at D47 and reported complete functional rescue following transplantation of D40 cells in QA lesioned mice, whereas Arber et al. (2015) used Activin signaling to produce DARPP32$^+$ cells at ~40% efficiency on D43 but did not observe behavioral improvement post transplantation of D20 cells in QA lesioned rats. In addition, Delli Carri et al. (2013) generated DARPP32$^+$ cells transcriptionally similar to those found in the brain at ~20% efficiency at D80, and demonstrated ~60% recovery in motor function (as tested by apomorphine-induced rotation) that lasted for a relatively modest 6 weeks after transplanting D38 cells in QA lesioned rats. While it is difficult to correlate treatment outcomes with the fraction of DARPP32$^+$ cells implanted, especially given the varying transplantation parameters between these studies, it is nonetheless apparent that DARPP32 levels solely may not be a predictive marker of CRT outcome (Arber et al., 2015; Aubry et al., 2008; Delli Carri et al., 2013; Ma et al., 2012). There is increasing evidence that a mixed population of striatal cells could be beneficial for alleviating HD symptoms (Rosser and Bachoud-Lévi, 2012), with recent work suggesting that glial cells in the striatum may play a pivotal role in HD (Benraiss et al., 2016). In addition, characterizing differentiated striatal populations via DARPP32 as well as other gene expression, and also using functional metrics, may be increasingly important. With this goal in mind, we used voltage-based imaging to evaluate the spiking characteristics of hPSC-derived striatal neurons quantitatively on a population level, thus incorporating a measure of functional maturation into our differentiation pipeline. Here, the hPSC-derived striatal population matured *in vitro* into ~40% DARPP32$^+$ neurons and ~27% glial cells, and 69% of all cells were shown to be spiking at D60.

hPSC-derived cells can be evaluated for their ability to improve function following transplantation into an animal model of disease. HD is a genetic disease characterized by progressive neurodegeneration, which occurs initially in the striatum and subsequently spreads to surrounding brain regions, correlating with gradual deterioration of motor and cognitive abilities (Walker, 2007). While chemical lesion models have contributed insights into the potential for striatal transplantations for treating HD (Arber et al., 2015; Aubry et al., 2008; Delli Carri et al., 2013; Ma et al., 2012), genetic models, including the R6/2 mouse, more closely match the progressive nature of the disease (Mangiarini et al., 1996). Previously, several different cell types were transplanted into the R6/2 striatum, including adipose-derived stem cells (Lee et al., 2009), neural stem cells (NSCs) (El Akabawy et al., 2012; Yang and Yu, 2009), NSC-derived striatal neurons (of which ~6% were DARPP32$^+$; El Akabawy et al., 2012), and mesenchymal stem cells (MSCs) (Rossignol et al., 2015). NSC and MSC transplantation provided short-term improvement, potentially via the secretion of neurotrophic factors (Lee et al., 2009; Rossignol et al., 2015). However, here graft integration following

transplantation of a defined hESC-derived striatal population offers promising, sustained functional improvement.

Cell survival is an important factor for functional enhancement but is likely more challenging to achieve following transplantation to a neurodegenerative environment compared with a chemically lesioned striatum. Accordingly, in some cases, as few as 100 of 450,000 cells have been reported to survive 6 weeks following striatal transplantation in R6/2 mice, a low survival rate that correlated with poor functional recovery (El Akabawy et al., 2012). In contrast, we found that ~5,700 of 100,000 transplanted cells survived 15 weeks after transplantation, with no signs of overgrowth. This increased survival could be due to transplantation of a more robust population of cells, which consisted of striatal MSN progenitors and glial cells. It is conceivable that survival of engrafted cells may have been even higher shortly after transplantation, and the neurodegenerative environment within the striatum and neighboring regions of the brain (the latter of which could lead to hindered axonal transport of beneficial neurotrophic factors to the striatum; Gauthier et al., 2004; Zuccato et al., 2001) could combine to compromise viability. Indeed, we observed nuclear-localized HTT aggregates in transplanted human neurons (Figure 4F), which may contribute to grafted cell death (Pecho-Vrieseling et al., 2014). Technologies to monitor cell survival, HTT transfer, and graft integration in real time would be beneficial. In addition, strategies to further enhance post-transplantation survival, for example with biomaterial cell delivery platforms (Adil et al., 2017b), or biomolecular intervention of HTT aggregation and transfer, may also be useful.

In conclusion, using an optimized differentiation protocol, we generated a functional hPSC-derived striatal population in a scalable 3D platform. The resulting population of cells comprised 43% DARPP32$^+$ neurons, of which 69% were electrophysiologically active cells, by D60. Striatal transplantation of these cells into the R6/2 mouse model of HD delayed disease onset, alleviated disease symptoms, and increased average lifespan by 19%. Moreover, ~6% of transplanted cells survived 12–15 weeks post transplantation and formed synaptic connections with surrounding host tissue. A defined 3D platform therefore offers strong potential for the scalable and efficient differentiation of therapeutically relevant cells to treat neurodegenerative disease.

EXPERIMENTAL PROCEDURES

Striatal Differentiation

H1 hESCs (WiCell), H9 hESCs (WiCell), or 8FLVY6C2 hiPSCs (gift from Dr. Joseph Wu; Lan et al., 2013) were differentiated to striatal progenitors on Matrigel-coated 2D surfaces (2D condition) or in PNIPAAm-PEG hydrogels (3D condition) for 26 days (Figure 1B). The 3D differentiation was initiated 5 days after single cell passage and maintenance in supplemented E8 medium with 10 μM ROCK inhibitor. Cells were exposed to Dual-SMAD inhibition using LDN193189 (100 nM; Stemgent) and SB431542 (10 μM; Selleckchem) for 5 days, followed by LDN193189 (100 nM) for an additional 5 days, either in DMEM-F12 (for condition M1 and M2) or in a 50:50 mixture of DMEM-F12 and Neurobasal medium (for M3) supplemented with 1:100 N2 (Life Technologies), 1:100 B27 (Life Technologies), and 1:100 Glutamax (Invitrogen) for 11 days. After D11, basal medium was switched to Neurobasal supplemented with 1:50 B27 and 1:100 Glutamax. To appropriately anteriorize the differentiating cell clusters, Wnt inhibitor DKK-1 (100 ng/mL; R&D Systems) was added to the culture from D2 to D26 (Delli Carri et al., 2013) for conditions M2 and M3. Similarly, to ventralize the cell clusters the SHH agonist purmorphamine (0.65 μM; Stemgent) was added from D2 to D26. In addition, the neurogenic factors BDNF (20 ng/mL; Peprotech), GDNF (20 ng/mL; Peprotech), dibutyryl-cAMP (1 μM; Santa Cruz Biotechnologies), and IGF1 (10 ng/mL; Peprotech) were used in media formulations from D15 onward (Ma et al., 2012). The 2D differentiation was initiated with >80% confluent hPSC cultures, and media formulations were followed as described above. Both 2D and 3D cultures were harvested at D26 and reseeded on 0.01% poly-L-ornithine (Sigma-Aldrich) and laminin (20 μg/mL; Life Technologies)-coated plates for continued culture.

Quantitative Immunocytochemistry

Cell clusters in the 3D platform were harvested by dissolving the gel in cold PBS, centrifuging, and re-suspending in 10 mM EDTA. Cells grown on 2D surfaces were harvested using EDTA. After pipet-mixing and dissociating the clusters down to ~100 μm in size, these smaller clusters were reseeded onto a 0.01% poly-L-ornithine (Sigma-Aldrich) and laminin (20 μg/mL; Invitrogen)-coated plate for 1 day in the relevant differentiation medium before fixing with 4% paraformaldehyde at the appropriate time point. Following three washes with PBS, one wash with 0.2% Triton in PBS, and one wash with 0.1% Triton in PBS, cells were blocked for 1 hr at room temperature on a rocker with primary blocking buffer (2% BSA, 5% donkey serum, 0.2% Triton X-100 in PBS). Primary antibodies diluted in primary blocking buffer were incubated with the cells overnight on a rocker at 4°C. The next day, cells were rinsed three times with PBS, followed by a 2 hr incubation with appropriate secondary antibodies diluted in 2% BSA in PBS. DAPI was added 30 min before the end of the secondary antibody incubation period. Cells were subsequently washed three times with PBS and imaged on a Zeiss AxioObserver fluorescent microscope. The primary and secondary antibodies used, and their respective dilutions, are presented in Table S1A. For the markers CALBINDIN and GABA, the numbers of cells labeled positive were counted in Cell Profiler and expressed as a percentage of total DAPI-labeled cells in the image. The percentage of cells positive for neuronal markers DARPP32 and CTIP2 were manually counted using the cell counter feature in ImageJ.

qPCR

At specified intervals during differentiation, cells were harvested and mRNA was extracted using a RNeasy Mini Kit (QIAGEN)

according to the manufacturer's instructions. mRNA was reverse-transcribed using iScript reverse transcriptase (Bio-Rad) and quantified using an iQ5 RT-PCR detection system (Bio-Rad). Data were normalized to GAPDH expression and analyzed using the $2^{\Delta\Delta Ct}$ method. The primers used for qPCR are presented in Table S1B.

Action Potential Analysis by Voltage-Sensitive Dyes

D26 striatal progenitors were harvested from 3D gels or from 2D Matrigel surfaces, seeded as small 50–100 μm clusters on laminin-coated 12 mm glass coverslips, and cultured using the differentiation medium described above. Voltage-sensitive dyes were used to monitor the electrophysiological activity of MSNs as previously described (Huang et al., 2015; Miller et al., 2012; Woodford et al., 2015). For experiments measuring spontaneous neuronal activity, the cells were incubated with 1 μM voltage-sensitive dye VoltageFluor in HBSS at 37°C for 15 min. Functional imaging of MSN cells was performed using a 20× objective paired with image capture from the ORCA-Flash4.0 camera (Hamamatsu) at a sampling rate of 100 Hz. VoltageFluor dye was excited using a 488 nm LED (light-emitting diode) with an intensity of 2.5 W/cm^2. For image analysis, a custom MATLAB routine (SpikeMapper, available upon request) was employed. Cells were selected by drawing regions of interest in a differential interference contrast image corresponding to the video and outputting the bleach-corrected trace as an Excel file. The spike times (measured as frames in which the intensity was greater than 3× the standard deviation of the overall trace) were outputted as a text file, and represented as spiking traces. For evoked activity experiments, cells were stimulated with a 1 ms, 60 V pulse from a trans-well stimulation electrode powered by a Grass SD9 Stimulator unit. Images were focused onto the ORCA-Flash4.0 using a 20× objective.

Cell Transplantation and Behavior Assays

All procedures in animals followed established NIH guidelines for animal care and use and were approved by the University of California, Berkeley, Animal Care and Use Committee (ACUC), the Committee for Laboratory and Environmental Biosafety (CLEB), and the Stem Cell Research Oversight committee (SCRO). Animals were placed in gender and pre-transplantation rotarod score matched groups, with group sizes determined using power analysis. All experimental and control animals were housed under the same conditions as approved by the Berkeley Office of Laboratory Animal Care (OLAC).

An H1 hESC-derived striatal population that was generated in PNIPAAm-PEG hydrogels using protocol M3 for 26 days, and subsequently matured on a 2D laminin-coated surface for 10 days, was harvested using 0.5 mM EDTA and manually mixed to generate small 50–100 μm clusters in Neurobasal medium (Invitrogen), and 100,000 cells in 2 μL were bilaterally injected into each striatum of 5 weeks postnatal R6/2 mice (Jackson, B6CBA-Tg(HDexon1)62Gpb/3J with 120 ± 5 CAG repeat units) at stereotaxic coordinates 0.50 mm AP, ± 1.75 mm medio-laterally (ML), and −2.0 mm dorso-ventrally (DV) using a Hamilton syringe. Starting 1 day before surgeries, mice were immunosuppressed with daily intraperitoneal injections of 10 mg/kg cyclosporine A for the duration of the experiment. Control mice that did not receive cells were similarly immunosuppressed. A separate cohort of 5-week-old wild-type mice, which were not part of the behavioral experimental group, were also transplanted with D35 MSNs to analyze graft morphology in a healthy brain.

Starting 2 weeks after striatal transplantations, at 7 weeks postnatal, disease progression in all animal groups was monitored weekly with the rotarod assay, clasping test, and weight measurements. For the rotarod assay, animals were placed onto a Rotamex-5 rotarod (Columbus Instruments), and their latency to fall (in seconds) was measured as the average of three of five trials, after discarding the highest and lowest scores. Each trial consisted of the rotarod accelerating from 4 to 40 rpm over 160 s. For the clasping test, mice were suspended by their tails for 30 s, and clasping behavior was scored between 0 and 3 as follows: 0, normal; 1, clasped hind limbs, but limbs are released within 30 s; 2, clasped hind limbs but recovers quickly only when released; 3, clasped hind limbs but failed to recover easily when released. Rotarod scores and weights were normalized to values at 7 weeks postnatal. End stage was determined when a clasping score of 3 was observed, or when mice reached 80% of their initial weight.

For retrograde labeling experiments, 2 μL of 2 w/v% Fluorogold (Santa Cruz Biotechnology) dissolved in 0.9% saline was injected into the substantia nigra of a subset of R6/2 animals with engrafted MSNs at stereotaxic coordinates −3 mm AP, ±1.2 mm ML, and −4.5 mm DV. Animals were sacrificed after 7 days for histology.

Histology and Immunohistochemistry

For histology, mice were sacrificed at 17–20 weeks postnatal using intracardiac perfusion with PBS followed by 4% paraformaldehyde. Brains were harvested and fixed in 4% paraformaldehyde overnight and transferred to 30% sucrose the following day. Following sufficient dehydration, brains were sectioned using a microtome to 40-μm-thick slices and stored in cryopreservation solution at −20°C. Following three washes with PBS, one wash with 0.2% Triton in PBS, and one wash with 0.1% Triton in PBS, sections were blocked for 1 hr at room temperature on a rocker with primary blocking buffer (2% BSA, 5% donkey serum, 0.2% Triton X-100 in PBS). Primary antibodies diluted in primary blocking buffer were incubated with the slide-mounted sections for 48 hr at 4°C. Next, sections were rinsed three times with PBS, followed by a 4 hr incubation with appropriate secondary antibodies diluted in 2% BSA in PBS. DAPI was added 30 min before the end of secondary antibody incubation period. Sections were subsequently washed three times with PBS and coverslipped with Fluoromount (Sigma-Aldrich). Sections were imaged on a Zeiss AxioObserver fluorescent microscope or on a Zeiss LSM 710 AxioObserver confocal microscope. The various primary and secondary antibodies used, and their respective dilutions, are presented in Table S1A. The percentages of cells positive for the HNA were manually counted using the cell counter feature in ImageJ, and total number of surviving cells were quantified using Abercrombie's principle (Abercrombie, 1946).

SUPPLEMENTAL INFORMATION

Supplemental Information includes four figures and one table and can be found with this article online at https://doi.org/10.1016/j.stemcr.2018.03.007.

AUTHOR CONTRIBUTIONS

M.M.A. and D.V.S. conceived the study. M.M.A. designed the experiments and performed the experiments with help from A.T.R. and G.N.R. T.G., with help from F.K.E., established the animal model. C.M.F. aided the transplantation. M.M.A. analyzed the data, with input from T.G. and A.T.R. R.U.K. performed the voltage-imaging experiments, and R.U.K. and E.W.M. analyzed the voltage-imaging data. M.M.A., T.G., and D.V.S. wrote the paper, with input from all authors.

ACKNOWLEDGMENTS

We thank Dr. A. Dillin for lending the rotarod apparatus and Dr. J.G. Flannery for providing space for behavioral studies. M.M.A. was supported in part by California Institute of Regenerative Medicine grants TG2-01164 and RT3-07800. T.G. was supported by a Ruth L. Kirschstein National Research Service Award (NRSA) (F32GM113446). R.U.K. was supported in part by an NIH training grant (GMT32GM066698). C.M.F. was supported in part by the NIH Stem Cell Biological Engineering Training Program (NIH T32GMP98218). E.W.M. acknowledges support from the NIH (R35GM119855 and R00NS078561), the Alzheimer's Association (2016-NIRG-394290), and the Alfred P. Sloan Foundation.

Received: January 30, 2017
Revised: March 7, 2018
Accepted: March 8, 2018
Published: April 5, 2018

REFERENCES

Abercrombie, M. (1946). Estimation of nuclear population from microtome sections. Anat. Rec. *94*, 239–247.

Adil, M.M., Rodrigues, G.M., Kulkarni, R.U., Rao, A.T., Chernavsky, N.E., Miller, E.W., and Schaffer, D.V. (2017a). Efficient generation of hPSC-derived midbrain dopaminergic neurons in a fully defined, scalable, 3D biomaterial platform. Sci. Rep. *7*, 40573.

Adil, M.M., Vazin, T., Ananthanarayanan, B., Rodrigues, G.M., Rao, A.T., Kulkarni, R.U., Miller, E.W., Kumar, S., and Schaffer, D.V. (2017b). Engineered hyaluronic acid hydrogels increase the post-transplantation survival of encapsulated hPSC-derived midbrain dopaminergic neurons. Biomaterials *136*, 1–11.

Arber, C., Precious, S.V., Cambray, S., Risner-Janiczek, J.R., Kelly, C., Noakes, Z., Fjodorova, M., Heuer, A., Ungless, M.A., Rodriguez, T.A., et al. (2015). Activin A directs striatal projection neuron differentiation of human pluripotent stem cells. Development *142*, 1375–1386.

Arlotta, P., Molyneaux, B.J., Jabaudon, D., Yoshida, Y., and Macklis, J.D. (2008). Ctip2 controls the differentiation of medium spiny neurons and the establishment of the cellular architecture of the striatum. J. Neurosci. *28*, 622–632.

Aubry, L., Bugi, A., Lefort, N., Rousseau, F., Peschanski, M., and Perrier, A.L. (2008). Striatal progenitors derived from human ES cells mature into DARPP32 neurons in vitro and in quinolinic acid-lesioned rats. Proc. Natl. Acad. Sci. USA *105*, 16707–16712.

Bachoud-Lévi, A.C., Gaura, V., Brugières, P., Lefaucheur, J.P., Boissé, M.F., Maison, P., Baudic, S., Ribeiro, M.J., Bourdet, C., Remy, P., et al. (2006). Effect of fetal neural transplants in patients with Huntington's disease 6 years after surgery: a long-term follow-up study. Lancet Neurol. *5*, 303–309.

Benraiss, A., Wang, S., Herrlinger, S., Li, X., Chandler-Militello, D., Mauceri, J., Burm, H.B., Toner, M., Osipovitch, M., Jim Xu, Q., et al. (2016). Human glia can both induce and rescue aspects of disease phenotype in Huntington disease. Nat. Commun. *7*, 11758.

Brewer, G.J., Torricelli, J.R., Evege, E.K., and Price, P.J. (1993). Optimized survival of hippocampal-neurons in B27-Supplemented neurobasal™, a new serum-free medium combination. J. Neurosci. Res. *35*, 567–576.

Carter, R.J., Lione, L.A., Humby, T., Mangiarini, L., Mahal, A., Bates, G.P., Dunnett, S.B., and Morton, A.J. (1999). Characterization of progressive motor deficits in mice transgenic for the human Huntington's disease mutation. J. Neurosci. *19*, 3248–3257.

Cepeda-Prado, E., Popp, S., Khan, U., Stefanov, D., Rodriguez, J., Menalled, L.B., Dow-Edwards, D., Small, S.A., and Moreno, H. (2012). R6/2 Huntington's disease mice develop early and progressive abnormal brain metabolism and seizures. J. Neurosci. *32*, 6456–6467.

Chen, C.S. (2016). 3D biomimetic cultures: the next platform for cell biology. Trends Cell Biol. *26*, 798–800.

Delli Carri, A., Onorati, M., Lelos, M.J., Castiglioni, V., Faedo, A., Menon, R., Camnasio, S., Vuono, R., Spaiardi, P., Talpo, F., et al. (2013). Developmentally coordinated extrinsic signals drive human pluripotent stem cell differentiation toward authentic DARPP-32+ medium-sized spiny neurons. Development *140*, 301–312.

Ehrlich, M.E. (2012). Huntington's disease and the striatal medium spiny neuron: cell-autonomous and non-cell-autonomous mechanisms of disease. Neurotherapeutics *9*, 270–284.

El Akabawy, G., Rattray, I., Johansson, S.M., Gale, R., Bates, G., and Modo, M. (2012). Implantation of undifferentiated and predifferentiated human neural stem cells in the R6/2 transgenic mouse model of Huntington's disease. BMC Neurosci. *13*, 97.

Foroud, T., Gray, J., Ivashina, J., and Conneally, P.M. (1999). Differences in duration of Huntington's disease based on age at onset. J. Neurol. Neurosurg. Psychiatry *66*, 52–56.

Gallina, P., Paganini, M., Lombardini, L., Mascalchi, M., Porfirio, B., Gadda, D., Marini, M., Pinzani, P., Salvianti, F., Crescioli, C., et al. (2010). Human striatal neuroblasts develop and build a striatal-like structure into the brain of Huntington's disease patients after transplantation. Exp. Neurol. *222*, 30–41.

Gauthier, L.R., Charrin, B.C., Borrell-Pagès, M., Dompierre, J.P., Rangone, H., Cordelières, F.P., De Mey, J., MacDonald, M.E., Lessmann, V., Humbert, S., et al. (2004). Huntingtin controls neurotrophic support and survival of neurons by enhancing BDNF vesicular transport along microtubules. Cell *118*, 127–138.

Gerecht, S., Burdick, J.A., Ferreira, L.S., Townsend, S.A., Langer, R., and Vunjak-Novakovic, G. (2007). Hyaluronic acid hydrogel for controlled self-renewal and differentiation of human embryonic stem cells. Proc. Natl. Acad. Sci. USA *104*, 11298–11303.

Huang, Y.L., Walker, A.S., and Miller, E.W. (2015). A photostable silicon rhodamine platform for optical voltage sensing. J. Am. Chem. Soc. *137*, 10767–10776.

Kirkeby, A., Grealish, S., Wolf, D.A., Nelander, J., Wood, J., Lundblad, M., Lindvall, O., and Parmar, M. (2012). Generation of regionally specified neural progenitors and functional neurons from human embryonic stem cells under defined conditions. Cell Rep. *1*, 703–714.

Kraehenbuehl, T.P., Langer, R., and Ferreira, L.S. (2011). Three-dimensional biomaterials for the study of human pluripotent stem cells. Nat. Methods *8*, 731–736.

Kriks, S., Shim, J.-W., Piao, J., Ganat, Y.M., Wakeman, D.R., Xie, Z., Carrillo-Reid, L., Auyeung, G., Antonacci, C., Buch, A., et al. (2011). Dopamine neurons derived from human ES cells efficiently engraft in animal models of Parkinson's disease. Nature *480*, 547–551.

Kulkarni, R.U., Yin, H., Pourmandi, N., James, F., Adil, M.M., Schaffer, D.V., Wang, Y., and Miller, E.W. (2017). A rationally-designed, general strategy for membrane orientation of photoinduced electron transfer-based voltage-sensitive dyes. ACS Chem. Biol. *12*, 407–413.

Lan, F., Lee, A.S., Liang, P., Sanchez-Freire, V., Nguyen, P.K., Wang, L., Han, L., Yen, M., Wang, Y., Sun, N., et al. (2013). Abnormal calcium handling properties underlie familial hypertrophic cardiomyopathy pathology in patient-specific induced pluripotent stem cells. Cell Stem Cell *12*, 101–113.

Lancaster, M.A., Renner, M., Martin, C.-A., Wenzel, D., Bicknell, L.S., Hurles, M.E., Homfray, T., Penninger, J.M., Jackson, A.P., and Knoblich, J.A. (2013). Cerebral organoids model human brain development and microcephaly. Nature *501*, 373–379.

Lee, S.T., Chu, K., Jung, K.H., Im, W.S., Park, J.E., Lim, H.C., Won, C.H., Shin, S.H., Lee, S.K., Kim, M., and Roh, J.K. (2009). Slowed progression in models of Huntington disease by adipose stem cell transplantation. Ann. Neurol. *66*, 671–681.

Lei, Y., and Schaffer, D.V. (2013). A fully defined and scalable 3D culture system for human pluripotent stem cell expansion and differentiation. Proc. Natl. Acad. Sci. USA *110*, E5039–E5048.

Li, J.Y., Popovic, N., and Brundin, P. (2005). The use of the R6 transgenic mouse models of Huntington's disease in attempts to develop novel therapeutic strategies. NeuroRx *2*, 447–464.

Lin, X., Shi, Y., Cao, Y., and Liu, W. (2016). Recent progress in stem cell differentiation directed by material and mechanical cues. Biomed. Mater. *11*, 014109.

Ma, L., Hu, B., Liu, Y., Vermilyea, S.C., Liu, H., Gao, L., Sun, Y., Zhang, X., and Zhang, S.C. (2012). Human embryonic stem cell-derived GABA neurons correct locomotion deficits in quinolinic acid-lesioned mice. Cell Stem Cell *10*, 455–464.

Mangiarini, L., Sathasivam, K., Seller, M., Cozens, B., Harper, A., Hetherington, C., Lawton, M., Trottier, Y., Lehrach, H., Davies, S.W., and Bates, G.P. (1996). Exon I of the HD gene with an expanded CAG repeat is sufficient to cause a progressive neurological phenotype in transgenic mice. Cell *87*, 493–506.

Miller, E.W., Lin, J.Y., Frady, E.P., Steinbach, P.A., Kristan, W.B., and Tsien, R.Y. (2012). Optically monitoring voltage in neurons by photo-induced electron transfer through molecular wires. Proc. Natl. Acad. Sci. USA *109*, 2114–2119.

Murphy, W.L., McDevitt, T.C., and Engler, A.J. (2014). Materials as stem cell regulators. Nat. Mater. *13*, 547–557.

Nakao, N., and Itakura, T. (2000). Fetal tissue transplants in animal models of Huntington's disease: the effects on damaged neuronal circuitry and behavioral deficits. Prog. Neurobiol. *61*, 313–338.

Pampaloni, F., Reynaud, E.G., and Stelzer, E.H.K. (2007). The third dimension bridges the gap between cell culture and live tissue. Nat. Rev. Mol. Cell Biol. *8*, 839–845.

Paul, B.D., Sbodio, J.I., Xu, R., Vandiver, M.S., Cha, J.Y., Snowman, A.M., and Snyder, S.H. (2014). Cystathionine γ-lyase deficiency mediates neurodegeneration in Huntington's disease. Nature *509*, 96–100.

Pecho-Vrieseling, E., Rieker, C., Fuchs, S., Bleckmann, D., Esposito, M.S., Botta, P., Goldstein, C., Bernhard, M., Galimberti, I., Müller, M., et al. (2014). Transneuronal propagation of mutant huntingtin contributes to non–cell autonomous pathology in neurons. Nat. Neurosci. *17*, 1064–1072.

Rodrigues, G.M.C., Gaj, T., Adil, M.M., Wahba, J., Rao, A.T., Lorbeer, F.K., Kulkarni, R.U., Diogo, M.M., Cabral, J.M.S., Miller, E.W., et al. (2017). Defined and scalable differentiation of human oligodendrocyte precursors from pluripotent stem cells in a 3D culture system. Stem Cell Reports *8*, 1770–1783.

Rosser, A.E., and Bachoud-Lévi, A.C. (2012). Clinical trials of neural transplantation in Huntington's disease. Prog. Brain Res. *200*, 345–371.

Rossignol, J., Fink, K.D., Crane, A.T., Davis, K.K., Bombard, M.C., Clerc, S., Bavar, A.M., Lowrance, S.A., Song, C., Witte, S., et al. (2015). Reductions in behavioral deficits and neuropathology in the R6/2 mouse model of Huntington's disease following transplantation of bone-marrow-derived mesenchymal stem cells is dependent on passage number. Stem Cell Res. Ther. *6*, 9.

Walker, F.O. (2007). Huntington's disease. Lancet *369*, 218–228.

Woodford, C.R., Frady, E.P., Smith, R.S., Morey, B., Canzi, G., Palida, S.F., Araneda, R.C., Kristan, W.B., Kubiak, C.P., Miller, E.W., and Tsien, R.Y. (2015). Improved PeT molecules for optically sensing voltage in neurons. J. Am. Chem. Soc. *137*, 1817–1824.

Yang, C.R., and Yu, R.K. (2009). Intracerebral transplantation of neural stem cells combined with trehalose ingestion alleviates pathology in a mouse model of Huntington's disease. J. Neurosci. Res. *87*, 26–33.

Yin, X., Mead, B.E., Safaee, H., Langer, R., Karp, J.M., and Levy, O. (2016). Engineering stem cell organoids. Cell Stem Cell *18*, 25–38.

Zuccato, C., Ciammola, A., Rigamonti, D., Leavitt, B.R., Goffredo, D., Conti, L., MacDonald, M.E., Timmusk, T., Sipione, S., and Cattaneo, E. (2001). Loss of huntingtin-mediated BDNF gene transcription in Huntington's disease. Science *293*, 493–498.